

## Investigation of band masses and $g$ values of ZnSe by two-photon magnetoabsorption

H. W. Hölscher, A. Nöthe, and Ch. Uihlein

*Institut für Physik, Universität Dortmund, 4600 Dortmund 50, Federal Republic of Germany*

(Received 23 April 1984)

We present two-photon magnetoabsorption measurements of the  $2P$ -exciton system in ZnSe. The measurements were carried out in Faraday ( $\vec{k} \parallel \vec{B}$ ) and Voigt configurations ( $\vec{k} \perp \vec{B}$ ) in fields up to 9 T. By various combinations of the polarization states of the two photons involved ( $\sigma_+, \sigma_-, \sigma, \pi$ ), up to 22 different magnetic substates can be selectively excited. The Zeeman splitting is highly nonlinear and critically dependent on the set of effective-mass parameters and  $g$  values. The large number of magnetic components allows a very precise determination of all relevant mass parameters ( $m_e^*, g_c, \gamma_1, \gamma_2, \gamma_3, \kappa$ ). The theoretical data presented in this paper are based on the effective-mass theory for degenerate bands and result from a numerical calculation of the eigenvalues of a set of coupled eigenvalue equations. The Hamiltonian describing the motion of electron and hole in the presence of an external magnetic field is fully expressed by means of spherical tensor operators.

### I. INTRODUCTION

In the last ten years there has been a controversial discussion of the correct numerical values of the band parameters of ZnSe. Most of them were deduced from experimental data of excitons. Especially the  $1S$  exciton has been studied in detail by several methods. Venghaus<sup>1</sup> and Feierabend and Weber<sup>2</sup> investigated the  $S$ -exciton spectra by magnetoreflexion. Recently Sermage and Fishman<sup>3</sup> reported experiments using resonant Brillouin scattering. Unfortunately the  $1S$ -exciton binding energy is not only affected by the complex valence band structure which is known to lead to a nonhydrogenic exciton series but also by a number of additional correction terms (exciton-photon, exciton-phonon, and exchange interaction) which are of similar importance. In particular, these measurements give only information about the reduced mass so that additional information about the effective mass of the conduction band is needed to get the complete set of mass parameters. The reliability of the valence-band parameters, therefore, depends critically on the accuracy of the conduction-band mass which has to be taken from some other independent experiments.<sup>4-7</sup> Magnetic field measurements on  $P$  excitons allow the simultaneous determination of all band masses since the linear Zeeman splitting of the  $P$  envelope is proportional to the difference of the reciprocal band masses ( $\gamma_e - \gamma_1$ ), whereas the diamagnetic shift depends on the sum ( $\gamma_e + \gamma_1$ ). The  $2P$  exciton was first investigated by Sondergeld and Stafford.<sup>8</sup> They found a pronounced fine structure with three distinct peaks due to the coupling between the angular momentum  $\vec{L}$  ( $L=1$ ) of the envelope and the hole spin  $\vec{J}$  ( $J=\frac{3}{2}$ ). The three coupled states of the  $2P$  exciton are highly degenerate and thus we expect a splitting in a magnetic field into 24 components. From the magnitude of the splitting one can calculate the Luttinger<sup>9</sup> parameters and  $g$  values.

The  $P$ -exciton states in ZnSe are not directly allowed for optical transitions. Two-photon absorption (TPA) spectroscopy, however, is an appropriate technique for investigations of the  $P$  exciton. It offers the possibility of a

selective excitation of substates with different magnetic quantum numbers by a suitable choice of the polarizations of the two light beams. Similar measurements on the less complicated exciton system in ZnO by Dinges *et al.*<sup>10</sup> and CdS by Damen *et al.*<sup>11</sup> and by Seiler *et al.*<sup>12</sup> have already demonstrated the advantages of this spectroscopic technique for investigations of excitonic fine structures. In our experiments we have resolved most of the 24 components of the  $2P$  exciton using magnetic fields up to 9 T. Owing to this large number of experimental data we can deduce the band masses and  $g$  values with much higher accuracy than before. Parameters are obtained from a comparison of our experimental data with numerical values calculated within the effective mass theory. Our magnetic field Hamiltonian contains full information about the complex valence-band structure in the vicinity of the  $\Gamma$  point. The eigenvalues are calculated variationally by an exact diagonalization in the appropriate subspace. We do not use a perturbational approach. The Hamiltonian describes the motion of the mutually interacting electron and hole in the presence of an external magnetic field within the axial approximation.

### II. EXPERIMENT

The two-photon magnetoabsorption measurements on the  $P$ -exciton fine structure of ZnSe were carried out with an experimental setup similar to that of Sondergeld and Stafford<sup>8</sup> described in detail in Ref. 13. As a high-power laser we use a Raman-shifted ( $H_2$  gas at 40 bars) Nd-doped YAG (yttrium aluminum garnet) laser which yields pulses up to 5 MW at 0.649 66 eV. The tunable laser consists of a dye oscillator (Rhodamine-6G) pumped by a YAG laser (second-harmonic of 1.06  $\mu\text{m}$  wavelength).

The two-photon signal  $I_\Delta$  is monitored as a change in transmission for the tunable dye laser (halfwidth 100 ns). As shown schematically in Fig. 1 the signal can be identified as a small dip on the dye laser pulse. This dip follows in its temporal behavior the short YAG laser pulse (halfwidth 7 ns). To detect the small absorption quantitatively we have applied a differential technique: The dye

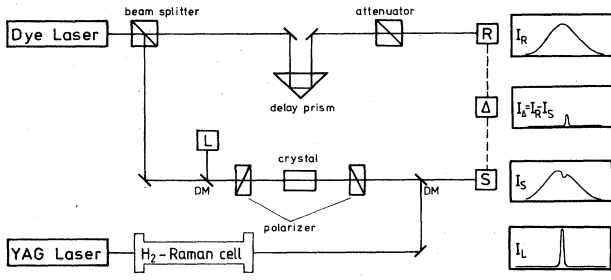


FIG. 1. Schematic diagram of the two-photon setup and the time dependence of the relevant signals; the high-power beam ( $I_L$ ) is positioned to be collinear with the signal beam ( $I_S$ ) by means of a dielectric mirror (DM).

laser output is split into two components (signal and reference beam). While the signal beam passes the crystal and is attenuated due to the two-photon absorption the reference beam bypasses the crystal. To assure that the difference between the electronic signals of the reference beam and the signal beam vanishes as long as the high-power laser is switched off, the delay time and the intensity of the reference beam is controlled by means of a delay prism and a variable attenuator. The two-photon absorption coefficient<sup>13</sup> is proportional to the nonlinear absorption signal  $I_\Delta = I_R - I_S$ .

For our magnetic field measurements we used the same polycrystalline sample as Sondergeld and Stafford.<sup>8</sup> The crystal is mounted in a helium cryostat with a superconducting coil allowing fields up to 9 T. The sample is thermally coupled to the liquid helium by low-pressure helium gas. The polarization states of the two laser beams can be changed automatically by rotating quarter-wave or half-wave plates. Because of different selection rules for the substates the measurements are performed in Faraday ( $\vec{k} \parallel \vec{B}$ ) and Voigt ( $\vec{k} \perp \vec{B}$ ) configuration.

### III. THEORY

In Sec. III A we will give a magnetic field Hamiltonian for excitons originating from a  $\Gamma_8$  valence band. The formalism is analogous to that of Altarelli and Lipari,<sup>14</sup> with the difference, that we use irreducible spherical tensor operators, which are easier to handle. In Sec. III B we will construct the eigenstates and derive the corresponding eigenvalue equations of the  $P$  excitons in a magnetic field. In the last part we will discuss the TPA selection rules in the axial model.

#### A. The magnetic field Hamiltonian

We present an effective mass Hamiltonian for excitons of degenerate bands in the presence of a magnetic field. Following Baldereschi and Lipari<sup>15</sup> and Altarelli and Lipari<sup>14</sup> we will write the Hamiltonian in the formalism of irreducible spherical tensor operators. By means of a finite-element technique we will exactly diagonalize the Hamiltonian in a suitable subspace to get the eigenvalues as functions of the band parameters.

ZnSe is a direct-band-gap material crystallizing in the

zinc-blende structure. The  $s$ -like  $\Gamma_6$  conduction band is twofold degenerate due to spin degeneracy. The upper valence band has  $\Gamma_8$  symmetry and is fourfold degenerate. The excitons originating from these band states have a binding energy which is about 25 times smaller than the spin-orbit splitting of the  $\Gamma_7$  and  $\Gamma_8$  valence bands which allows to neglect the influence of the split off  $\Gamma_7$  valence band. Since the  $P$  excitons in ZnSe are not dipole allowed, we do not have to take into account their coupling to the radiation field. Contrary to investigations of  $S$  excitons we do not have to include central-cell corrections<sup>16</sup> because  $P$  excitons have a more extended wave function with a zero at the origin.

As was shown by Baldereschi and Lipari<sup>15</sup> the Hamiltonian consists of the following three terms:

$$H = H_s + H_{d,\text{sph}} + H_{d,\text{cub}}, \quad (1a)$$

$$H_s = \frac{P^2}{\hbar^2} - \frac{2}{r}, \quad (1b)$$

$$H_{d,\text{sph}} = -\frac{\mu}{9\hbar^2} (P^{(2)} \cdot J^{(2)}), \quad (1c)$$

$$H_{d,\text{cub}} = \frac{\delta}{9\hbar^2} \left[ [P^{(2)} \times J^{(2)}]_{+4}^{(4)} + \frac{\sqrt{70}}{5} [P^{(2)} \times J^{(2)}]_0^{(4)} + [P^{(2)} \times J^{(2)}]_{-4}^{(4)} \right], \quad (1d)$$

$$\mu = \frac{6\gamma_3 + 4\gamma_2}{5(\gamma_e + \gamma_1)}, \quad \delta = \frac{\gamma_3 - \gamma_2}{\gamma_e + \gamma_1}.$$

The parameters  $\gamma_1$ ,  $\gamma_2$ , and  $\gamma_3$  are the Luttinger parameters of the  $\Gamma_8$  valence band. The  $\Gamma_6$  conduction band is described by  $\gamma_e = m_0/m_e^*$ . Energies and lengths are expressed in units of the effective Rydberg and the exciton Bohr radius:

$$R_{\text{eff}} = \frac{1}{(\gamma_e + \gamma_1)\epsilon^2} R_H,$$

$$a_{\text{ex}} = (\gamma_e + \gamma_1)\epsilon a_B$$

The  $H_d$  terms represent a coupling between the angular momentum of the electron-hole motion and the hole spin. This interaction is given in the form of scalar and tensor products of the irreducible spherical tensor operators<sup>15</sup>  $P^{(2)}$  and  $J^{(2)}$ . We include into the Hamiltonian the effects of an external magnetic field by substituting the operator  $\vec{p}$  of the momentum by the canonical momentum  $\vec{p} - (e/c)\vec{A}$ .

We choose for the magnetic field the gauge  $\vec{A} = \frac{1}{2}(\vec{B} \times \vec{r})$  with  $\vec{B} = (0, 0, B)$ . From the  $H_s$  term two parts arise which depend linearly or quadratically on the magnetic field  $B$ :

$$H_{s,\text{mag}} = H_s + H_{s,1} + H_{s,\text{dia}}, \quad (2a)$$

$$H_{s,1} = \mu_B B (\gamma_e - \gamma_1) L_z + \mu_B B g_c S_z - 2\mu_B B \kappa J_z, \quad (2b)$$

$$H_{s,\text{dia}} = \frac{1}{4} \mu_B^2 B^2 (\gamma_e + \gamma_1)^2 (x^2 + y^2). \quad (2c)$$

The Zeeman term of the envelope is proportional to the difference of the reciprocal band masses of the conduction

and the valence band. This part is characteristic for the magnetic field behavior of  $P$  excitons since it represents the significant splitting into three components according to the projection of the angular momentum on the axis of the magnetic field.  $S$  excitons cannot show this splitting because the angular momentum is zero. In the  $H_{s,1}$  term we have furthermore considered the Zeeman term associated with the electron and hole spin. The diamagnetic shift, given by  $H_{s,\text{dia}}$ , depends quadratically on the mag-

netic field and the sum of the reciprocal band masses. In the presence of an external magnetic field the cubic  $H_d$  term becomes partially quenched. For this reason we consider in the following only axial contributions to the Hamiltonian. The spherical and the axial  $H_d$  terms are of the same structure besides numerical factors, which depend only on the difference in the magnetic quantum number  $M_L$ . These factors are given in the Appendix. The spherical  $H_d$  term consists of the following terms:

$$H_{d,1} = -\frac{i}{9}(\gamma_e + \gamma_1)\mu\sqrt{5/6}\mu_B B \{[(\mathbf{R}^{(1)} \times \mathbf{P}^{(1)})^{(1)} \times \mathbf{J}^{(2)}]_0^{(1)} - \sqrt{3}[(\mathbf{R}^{(1)} \times \mathbf{P}^{(1)})^{(2)} \times \mathbf{J}^{(2)}]_0^{(1)}\}, \quad (3)$$

$$H_{d,\text{dia}} = \frac{1}{108}(\gamma_e + \gamma_1)^2\mu\mu_B^2 B^2 \{ \mathbf{R}^{(2)} \cdot \mathbf{J}^{(2)} + \sqrt{14}[\mathbf{R}^{(2)} \times \mathbf{J}^{(2)}]_0^{(2)} + \sqrt{2/3}r^2 \mathbf{J}_0^{(2)} \}. \quad (4)$$

Similar to the  $H_s$  term there are also two magnetic contributions. The first is linear in  $B$  and can be compared to the Zeeman term, whereas the second is a diamagnetic term, which depends quadratically on the magnetic field. Both parts depend on the spherical parameter  $\mu$  as well as on the sum of the reciprocal band masses ( $\gamma_e + \gamma_1$ ). These additional terms in the Hamiltonian describe the effects of the complex valence-band structure on the magnetic field behavior of the  $2P$  excitons. We want to emphasize that our Hamiltonian, which includes the axial contributions of the cubic term, is equivalent to the Hamiltonian given by Altarelli and Lipari<sup>14</sup> in terms of Cartesian tensor operators. Contrary to the case, where one uses Cartesian operators, the evaluation of matrix elements using spherical tensor operators is simple and can be done very easily by using the Wigner-Eckart theorem<sup>17</sup> and applying the technique of reduced matrix elements. We have listed the reduced matrix elements for all operators in the Appendix. By means of  $6j$  and  $9j$  symbols the reduced matrix elements of tensor products can be deduced from those of the operators themselves.

### B. Construction of eigenstates and eigenvalue equations

In high magnetic fields the  $2P$  exciton splits into 24 magnetic substates. In order to understand this complex splitting pattern we will first construct the eigenstates of the coupled envelope-hole system without external perturbation. Then we will include the magnetic field and discuss the behavior of the excitonic states in the axial approximation described above. Within the spherical model the  $2P$  exciton, being composed of a  $p$ -like envelope ( $L=1$ ),  $\Gamma_8$  valence-band states ( $J=\frac{3}{2}$ ), and  $\Gamma_6$  conduction-band states ( $S=\frac{1}{2}$ ), splits into three envelope-hole coupled states  $P_F$  with  $F=\frac{1}{2}, \frac{3}{2},$  and  $\frac{5}{2}$  ( $\vec{F}=\vec{L}+\vec{J}$ ). Since the coupling between the electron spin  $\vec{S}$  and the angular momentum  $\vec{F}$  is negligible, the electron spin can be separated. We have to keep in mind, however, that the electron spin doubles the degeneracy of the excitonic states  $P_F$ . In the presence of an external magnetic field an additional Zeeman splitting due to the electron  $g$  value ( $g_e$ ) is thus to be expected. The spherical  $H_d$  term couples states with the same angular momentum  $\vec{F}$ . In a magnetic field, states with different angular momentum  $\vec{F}$

will be mixed. The magnetic quantum number  $M_F$ , however, remains a good quantum number. Thus the eigenstates in the presence of an external magnetic field can be written as linear combinations of product functions:

$$|M_F, M_S\rangle = \sum_{L,F} g_{LF}(r) |L, J, F, M_F\rangle |S, M_S\rangle. \quad (5)$$

The  $g_{LF}(r)$  are radial functions and the  $|L, J, F, M_F\rangle$  and  $|S, M_S\rangle$  are angle- and spin-dependent parts defined in the coupling scheme as mentioned before. For the calculation of the magnetic field dependence of a state  $|M_F, M_S\rangle$  one has to include correctly all states with the same magnetic quantum number. For an exciton in a magnetic field, parity is still a good quantum number. Therefore, only states with odd angular momentum ( $L=3, 5, 7, \dots$ ) are mixed to the  $P$  excitons. For our numerical calculations we have included only  $f$ -like states ( $L=3$ ) neglecting contributions from excitons with higher angular momenta. The coupling scheme for the

TABLE I. Construction of  $M_{\text{tot}}$  from the magnetic quantum numbers of the envelope  $M_L$ , of the hole spin  $M_J$ , and of the electron spin  $M_S$ ; in the general case only  $M_F=M_L+M_J$  and  $M_S$  are good quantum numbers, but in the limiting case of the excitonic Paschen-Back effect the magnetic substates can be classified by  $M_L$ ,  $M_J$ , and  $M_S$  themselves.

$M_F$	$M_L$	$M_J$	$M_S$	$M_{\text{tot}}$
$\frac{5}{2}$	1	$\frac{3}{2}$	$\frac{1}{2}$	3
$\frac{5}{2}$	1	$\frac{3}{2}$	$-\frac{1}{2}$	2
$\frac{3}{2}$	0	$\frac{3}{2}$	$\frac{1}{2}$	2
$\frac{3}{2}$	0	$\frac{3}{2}$	$-\frac{1}{2}$	1
$\frac{3}{2}$	1	$\frac{1}{2}$	$\frac{1}{2}$	2
$\frac{3}{2}$	1	$\frac{1}{2}$	$-\frac{1}{2}$	1
$\frac{1}{2}$	-1	$\frac{3}{2}$	$\frac{1}{2}$	1
$\frac{1}{2}$	-1	$\frac{3}{2}$	$-\frac{1}{2}$	0
$\frac{1}{2}$	0	$\frac{1}{2}$	$\frac{1}{2}$	1
$\frac{1}{2}$	0	$\frac{1}{2}$	$-\frac{1}{2}$	0
$\frac{1}{2}$	1	$-\frac{1}{2}$	$\frac{1}{2}$	1
$\frac{1}{2}$	1	$-\frac{1}{2}$	$-\frac{1}{2}$	0

magnetic substates is given in Table I. Within this coupling scheme we have solved the angular part of the eigenvalue problem analytically as is demonstrated in the Appendix. The resulting systems of radial differential equations are treated numerically by the finite element method. The numerical calculations were performed in the same way as described by Mattausch and Uihlein.<sup>18</sup> We want to point out that we have solved the eigenvalue equations numerically exactly within the axial model. The energetic levels of the magnetic substates depend on the set of free parameters  $\gamma_1, \gamma_2, \gamma_3, m_e^*, g_e, \kappa$ , and  $R_{\text{eff}}$  and can be fitted to the experimental results as discussed later.

### C. Two-photon absorption selection rules in an axial model

The two-photon selection rules follow from a consideration of a combination of two one-photon absorption processes, each of which gives rise to a change of the magnetic quantum number by 0 or  $\pm 1$ . Depending on the polarization directions of both lasers one gets different selection rules: In Faraday configuration ( $\vec{k} \parallel \vec{B}$ ) circularly polarized light is used which leads to transitions into states with total magnetic quantum number  $M_{\text{tot}} = 0$  and  $\pm 2$ . It should be noted, that the selection rules only depend on the helicity of the electric field vector with respect to the magnetic field. Working with two circularly polarized beams of opposite helicity one can excite states with  $M_{\text{tot}} = 0$ . With two beams of the same helicity transitions into magnetic substates with  $M_{\text{tot}} = \pm 2$  are possible. Additional measurements in Voigt configuration ( $\vec{k} \perp \vec{B}$ ) with linearly polarized light allow the observation of states with  $M_{\text{tot}} = 0, \pm 1$ , and  $\pm 2$ . The polarization axis of linearly polarized light is oriented either parallel ( $\pi$ ) or perpendicular ( $\sigma$ ) to the magnetic field. States with  $M_{\text{tot}} = \pm 1$  are excited by a combination of  $\pi$ - and  $\sigma$ -polarized light. If the directions of the polarizations of the two photons are parallel there are two possibilities: If they are polarized parallel to the magnetic field  $\vec{B}$ , transitions to  $M_{\text{tot}} = 0$ , and if they are perpendicular to  $\vec{B}$ , transitions to  $M_{\text{tot}} = 0$  and  $\pm 2$  are possible. The different combinations are listed in Table II.

TABLE II. Two-photon selection rules in the axial model; the first sign refers to the polarization of the dye laser, the second to the high power YAG laser.

Polarization state	$M_{\text{tot}}$	
$\vec{k} \parallel \vec{B}$	$\sigma_+ \sigma_+$	2
	$\sigma_+ \sigma_-$	0
	$\sigma_- \sigma_+$	0
	$\sigma_- \sigma_-$	-2
$\vec{k} \perp \vec{B}$	$\sigma \sigma$	0, $\pm 2$
	$\sigma \pi$	$\pm 1$
	$\pi \sigma$	$\pm 1$
	$\pi \pi$	0

## IV. EXPERIMENTAL RESULTS

In this section we will present our two-photon results for ZnSe.<sup>19</sup> The experimental results are compared to energy values calculated within the preceding model using the best set of parameters. We investigated the  $2P$ -exciton fine structure in magnetic fields up to 9 T with eight different polarization combinations in Faraday and Voigt configuration, respectively. Figure 2 shows a typical series of measurements in Faraday configuration. Owing to the helicity of the photons relative to the magnetic field ( $\sigma_+, \sigma_-$ ) only transitions to states with  $M_{\text{tot}} = 0$  are allowed. It is seen that the magnetic fine structure of the  $2P$  exciton strongly depends on the magnitude of the magnetic field. At 8 T the magnetic-field-induced splitting of 5 meV is considerably larger than the initial splitting due to the envelope-hole coupling (1.7 meV). The separation of the spectra into three principal structures at high magnetic fields suggests that the dominant splitting is determined by the orientation of the angular momentum of the electron-hole motion ( $M_L = -1, 0, +1$ ). This means that the coupling of the angular momentum  $\vec{L}$  to the magnetic field is much stronger than the coupling to

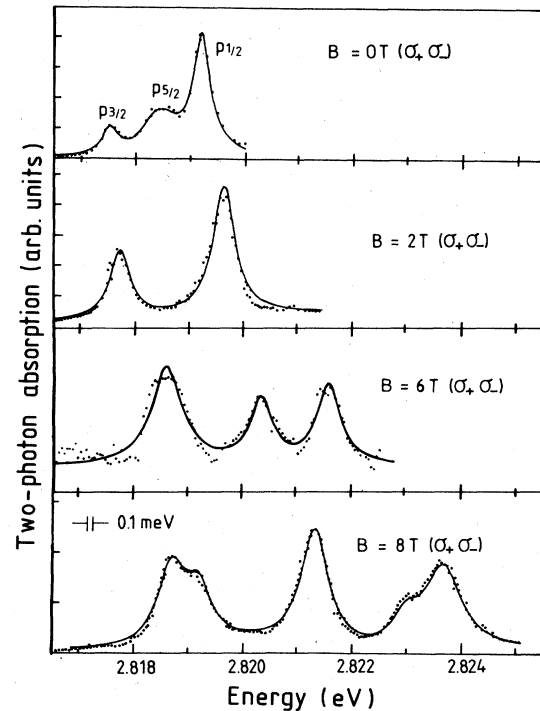


FIG. 2. Two-photon absorption measurements of the  $2P$  exciton in Faraday configuration up to 8 T with  $(\sigma_+, \sigma_-)$  polarization; the first sign refers to the polarization of the dye laser, the second to the high power YAG laser; in the upper panel the fine structure is shown for the field-free case. The lines result from a line-shape fit using up to six Lorentz functions.

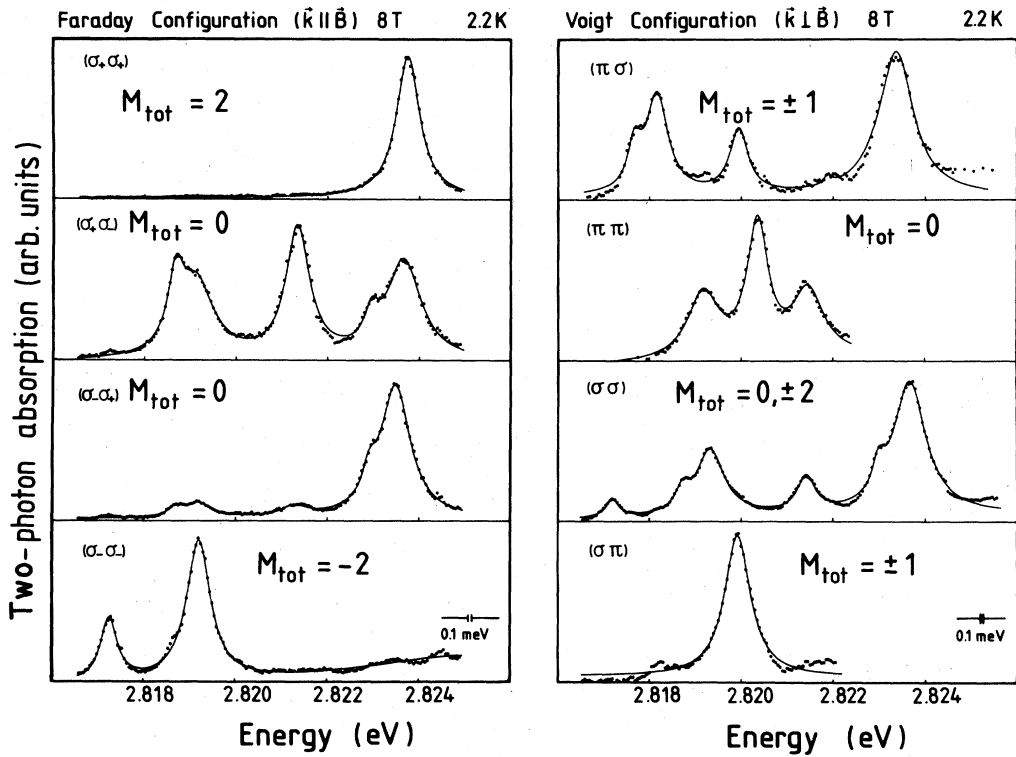


FIG. 3.  $2P$ -exciton fine structure at 8 T for the eight different polarization states of the two beams in Faraday (left) and Voigt configuration (right).

the hole spin  $\vec{J}$ , which can be interpreted as an excitonic Paschen-Back effect. In Fig. 3 the TPA spectra at 8 T are shown for all possible polarization configurations. The possibility of selective excitation allows to distinguish between the various states. A calculation of the two-photon oscillator strengths gives an unambiguous assignment of the peaks. All experimental results are summarized in Fig. 4. The experimental results (dots) are compared to the energy values (lines) calculated within the axial model using the best set of parameters. The number of excitonic

states exceeds the number of free parameters. Thus an unambiguous determination of the parameters is possible. Fitting the theoretical values to the experimental results for all measurements up to 9 T we receive a reliable set of parameters:

$$m_e^* = (0.147 \pm 0.003)m_0,$$

$$\gamma_1 = 2.45 \pm 0.05,$$

$$\gamma_2 = 0.61 \pm 0.12,$$

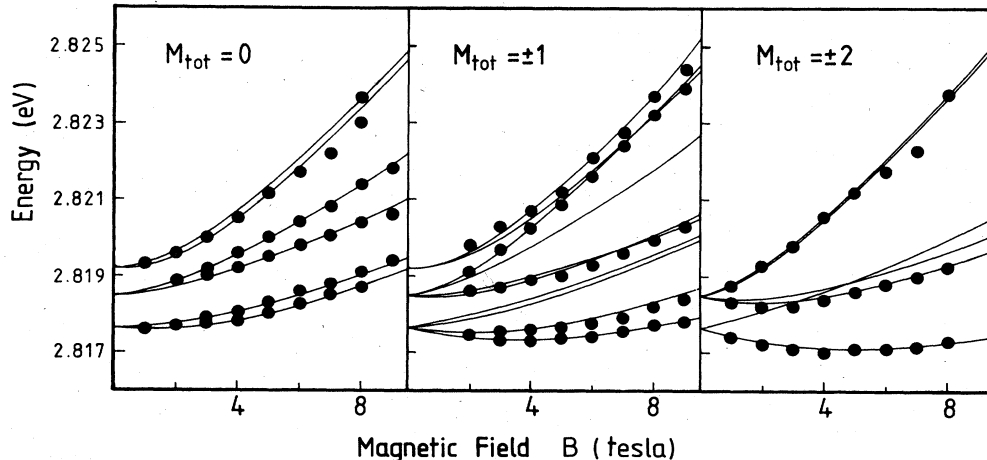


FIG. 4. Magnetic field dependence of the  $2P$  multiplet; lines: theoretical results, dots: experimental results.

$$\gamma_3 = 1.11 \pm 0.10,$$

$$g_c = 0.96 \pm 0.06,$$

$$\kappa = 0.20 \pm 0.04,$$

$$R_{\text{eff}} = 17.35 \pm 0.6 \text{ meV}.$$

The procedure of fitting the parameters is particularly sensitive to  $m_e^*$  and  $\gamma_1$ , so that they can be determined with very small errors. The difference of the Luttinger parameters  $\gamma_2$  and  $\gamma_3$  is deduced from the zero-field splitting of the  $P_{5/2}$  exciton into a  $\Gamma_7$  and a  $\Gamma_8$  component.

Using our set of parameters we have calculated the relative TPA-oscillator strengths for different magnetic fields and polarization configurations. The agreement with the experimental data is a justification of the axial model and gives further confidence in the evaluated set of parameters. The fact that some of the states listed in Table I are not observed in the experiments can be understood because of vanishing oscillator strength.

## V. DISCUSSION

The strong magnetic field dependence of the  $2P$ -exciton fine structure in the TPA spectra of ZnSe reveals information about the complex structure at the top of the  $\Gamma_8$  valence band. Besides the valence-band parameters one can deduce from our measurements the effective mass of the conduction band, the  $g$  values of electron and hole, and the Rydberg energy of the exciton series. In this section we will discuss the advantages of investigations of the  $P$  excitons in contrast to measurements of the  $S$ -exciton series. We will compare our parameters with data published by other authors (Table III).

As we have pointed out in the Introduction investigations of ZnSe concerning the fundamental gap were mostly performed on the excitonic ground state, i.e., the  $1S$  exciton. In this case one has to take into account that the  $1S$  exciton is strongly coupled to the photons which leads to polaritons. The polariton dispersion was investigated by Sermage and Fishman<sup>3</sup> using resonant Brillouin

scattering.  $S$  excitons are also affected by the exchange interaction, which enforces a splitting between the  $F_{\text{tot}} = 1$  and 2 components without any additional external perturbation. In one-photon experiments only the  $F_{\text{tot}} = 1$  component can be observed. Therefore, it is very difficult to deduce the strength of the exchange interaction. The  $F_{\text{tot}} = 2$  state becomes allowed in a high magnetic field and can be extrapolated to the field free case. For the case of the  $S$  exciton one can only see a diamagnetic shift and a small splitting due to the electron and hole spin. The magnetic field behavior of the  $S$  exciton in ZnSe was investigated by Feierabend and Weber<sup>2</sup> and by Venghaus<sup>1</sup> with magnetoreflexion measurements.

For determination of the band parameters Feierabend and Weber included the exciton-photon interaction, whereas Venghaus took polaron effects into account. Since the diamagnetic shift depends only on the sum of the reciprocal band masses, in both papers the authors had to assume a numerical value for the conduction-band mass to get the mean mass of the valence band described by the Luttinger parameter  $\gamma_1$ . Contrary to these measurements of  $S$  excitons we get an appreciable splitting of the  $P$  envelope, which depends on the difference of the reciprocal band masses ( $\gamma_e - \gamma_1$ ). From both, the diamagnetic shift and the envelope Zeeman splitting, we can deduce the conduction- and valence-band masses. The numerical values of the conduction-band mass from other authors range from  $0.13m_0$  to  $0.17m_0$  with an error of approximately 15%. From our measurements we derive  $m_e^* = 0.147$  with an accuracy of 2%. It is obvious, that the sets of parameters given by Feierabend and Weber<sup>2</sup> and by Venghaus<sup>1</sup> are influenced by their models and the special choice of the conduction-band mass. Sondergeld and Stafford<sup>8</sup> measured the  $2P$ -exciton fine structure of ZnSe without any external perturbation. For the determination of the valence-band parameters from the fine structure they also had to assume values for the conduction-band mass and the effective Rydberg energy. Finally we want to point out again that our parameter set gives a consistent description of all the features observed in our experiments, explaining the  $2P$ -exciton fine struc-

TABLE III. Comparison of our numerical results with data published by other authors.

	$m_e^*$	$\gamma_1$	$\gamma_2$	$\gamma_3$	$g_c$	$\kappa$	$R_{\text{eff}}$ (meV)
This paper	0.147	2.45	0.61	1.11	0.96	0.20	17.35
Venghaus (Ref. 1)		4.3	0.59	1.34	1.37	-0.28	16.8
Feierabend and Weber (Ref. 2)		4.32	0.66	1.13	1.2	-0.12	19.1
Sermage and Fishman (Ref. 3)		4.30	1.14	1.84			
Aven and Segall (Ref. 4)	0.15						
Segall and Marple (Ref. 5)	0.16						
Marple (Ref. 6)	0.17						
Wang and Klein (Ref. 7)	0.13						
Sondergeld and Stafford (Ref. 8)		3.23	0.69	0.90			19.9
Lawaetz (Ref. 20)		3.77	1.24	1.67			
Dunstan <i>et al.</i> (Ref. 21)					1.115		
Cavenett and Hagston (Ref. 22)					1.22	-0.20	

ture and the magnetic field behavior of it. The experiments on  $S$  excitons should be reinterpreted with particular consideration of the conduction-band mass given in this paper.

## VI. SUMMARY

The  $2P$ -exciton system is characterized by a high orbital- and spin-degeneracy which is as a result of the symmetry properties of the valence band partially lifted by the presence of an effective spin-orbit interaction. The Zeeman splitting of the  $2P$  exciton is highly nonlinear and depends sensitively on the ratio between Zeeman terms, diamagnetic terms, and the magnitude of the initial spin-orbit splitting. The Zeeman splitting of the  $2P$ -exciton system depends in fact so critically on the choice of the effective-mass parameters that the good agreement between experiment and theory is not only a rigorous test for the liability of the presented mass parameters but also an excellent proof for the validity of the effective mass approximation in the presence of a highly degenerate valence band.

## ACKNOWLEDGMENTS

The authors are grateful to D. Fröhlich for his continuous support of this work.

## APPENDIX

As an example we demonstrate the determination of the eigenstates for the  $M_F = +\frac{5}{2}$  states. The derivation follows the procedure of Baldereschi and Lipari<sup>15</sup> using irreducible spherical tensor operators. The eigenfunctions of the Hamiltonian described above are constructed in the following manner:

$$|M_F, M_s\rangle = \sum_{L,F} g_{LF}(r) |L, J, F, M_F\rangle |S, M_s\rangle. \quad (\text{A1})$$

For the  $M_F = \frac{5}{2}$  states there are four contributions:

- (1)  $L = 1, J = \frac{3}{2}, M_L = 1, M_J = \frac{3}{2}$ .
- (2)  $L = 3, J = \frac{3}{2}, M_L = 1, M_J = \frac{3}{2}$ .
- (3)  $L = 3, J = \frac{3}{2}, M_L = 2, M_J = \frac{1}{2}$ .
- (4)  $L = 3, J = \frac{3}{2}, M_L = 3, M_J = -\frac{1}{2}$ .

The matrix elements of the Hamiltonian can be calculated with the reduced matrix element technique using the Wigner-Eckart theorem.<sup>17</sup> The residual radial differential equations can be solved numerically by the finite-element method as discussed by Mattausch and Uihlein.<sup>18</sup> For the matrix elements we get

$$H_s + H_{d,\text{sph}} = \begin{pmatrix} -\left[1 + \frac{\mu}{5}\right]P_{11} - \frac{2}{r} & \frac{6}{5}\sqrt{1/14}\mu P_{13} & -\frac{6}{5}\sqrt{5/21}\mu P_{13} & \frac{6}{5}\sqrt{5/14}\mu P_{13} \\ \frac{6}{5}\sqrt{1/14}\mu P_{31} & -\left[1 - \frac{\mu}{5}\right]P_{33} - \frac{2}{r} & -\frac{1}{3}\sqrt{6/5}\mu P_{33} & -\frac{2}{3}\sqrt{1/5}\mu P_{33} \\ -\frac{6}{5}\sqrt{5/21}\mu P_{31} & -\frac{1}{3}\sqrt{6/5}\mu P_{33} & -P_{33} - \frac{2}{r} & 0 \\ \frac{6}{5}\sqrt{5/14}\mu P_{31} & -\frac{2}{3}\sqrt{1/5}\mu P_{33} & 0 & -\left[1 + \frac{\mu}{3}\right]P_{33} - \frac{2}{r} \end{pmatrix} \quad (\text{A2})$$

with

$$P_{11} = \frac{d^2}{dr^2} + \frac{2}{r} \frac{d}{dr} - \frac{2}{r^2},$$

$$P_{13} = \frac{d^2}{dr^2} + \frac{7}{r} \frac{d}{dr} + \frac{8}{r^2},$$

$$P_{31} = \frac{d^2}{dr^2} - \frac{3}{r} \frac{d}{dr} + \frac{3}{r^2},$$

$$P_{33} = \frac{d^2}{dr^2} + \frac{2}{r} \frac{d}{dr} - \frac{12}{r^2},$$

$$H_{s,\text{dia}} = \frac{(\gamma_e + \gamma_1)^2 \mu_B^2 B^2}{R_{\text{eff}}} r^2 \begin{pmatrix} \frac{1}{5} & -\frac{1}{10}\sqrt{2/7} & 0 & 0 \\ -\frac{1}{10}\sqrt{2/7} & \frac{2}{15} & 0 & 0 \\ 0 & 0 & \frac{1}{6} & 0 \\ 0 & 0 & 0 & \frac{2}{9} \end{pmatrix}, \quad (\text{A4})$$

$$H_{s,1} = \mu_B B \begin{pmatrix} (\gamma_e - \gamma_1) - 3\kappa - \frac{1}{2}g_c & 0 & 0 & 0 \\ 0 & (\gamma_e - \gamma_1) - 3\kappa - \frac{1}{2}g_c & 0 & 0 \\ 0 & 0 & 2(\gamma_e - \gamma_1) - \kappa - \frac{1}{2}g_c & 0 \\ 0 & 0 & 0 & 3(\gamma_e - \gamma_1) + \kappa - \frac{1}{2}g_c \end{pmatrix}, \quad (\text{A5})$$

$$H_{d,1} = (\gamma_e + \gamma_1) \mu_B B \begin{pmatrix} -\frac{1}{2} & 0 & \sqrt{3/35}K_{13} & -3\sqrt{2/35}K_{13} \\ 0 & -\frac{1}{2} & -\frac{3}{2}\sqrt{5/6} + \frac{1}{12}\sqrt{6/5}K_{33} & \frac{1}{3}\sqrt{1/5}K_{33} \\ \sqrt{3/35}K_{31} & -\frac{3}{2}\sqrt{5/6} - \frac{1}{12}\sqrt{6/5}K_{33} & 1 & 0 \\ -3\sqrt{2/35}K_{31} & -\frac{1}{3}\sqrt{1/5}K_{33} & 0 & \frac{3}{2} \end{pmatrix}, \quad (\text{A6})$$

with

$$\begin{aligned} K_{11} &= 3 + 2r \frac{d}{dr}, \\ K_{13} &= 4 + r \frac{d}{dr}, \\ K_{31} &= 1 - r \frac{d}{dr}, \\ K_{33} &= 3 + 2r \frac{d}{dr}, \end{aligned} \quad (\text{A7})$$

$$H_{d,\text{dia}} = \frac{(\gamma_e + \gamma_1)^2}{R_{\text{eff}}} \mu r^2 \mu_B^2 B^2 \begin{pmatrix} \frac{1}{10} & -\frac{1}{20}\sqrt{2/7} & 0 & \frac{3}{4}\sqrt{2/35} \\ -\frac{1}{20}\sqrt{2/7} & \frac{1}{15} & 0 & -6\sqrt{1/5} \\ 0 & 0 & -\frac{1}{12} & 0 \\ \frac{3}{4}\sqrt{2/35} & -6\sqrt{1/5} & 0 & -\frac{1}{9} \end{pmatrix}. \quad (\text{A8})$$

For the calculation we have used the following reduced matrix elements:

$$\begin{aligned} \langle L=1 | |[\underline{R}^{(1)} \times \underline{R}^{(1)}]^{(2)} | | L=1 \rangle &= i 3\sqrt{1/5} \left[ 3 + 2r \frac{d}{dr} \right], \\ \langle L=1 | |[\underline{R}^{(1)} \times \underline{R}^{(1)}]^{(2)} | | L=3 \rangle &= -i 3\sqrt{6/5} \left[ 4 + r \frac{d}{dr} \right], \\ \langle L=3 | |[\underline{R}^{(1)} \times \underline{R}^{(1)}]^{(2)} | | L=1 \rangle &= i 3\sqrt{6/5} \left[ 1 - r \frac{d}{dr} \right], \\ \langle L=3 | |[\underline{R}^{(1)} \times \underline{R}^{(1)}]^{(2)} | | L=3 \rangle &= -i\sqrt{14/5} \left[ 3 + 2r \frac{d}{dr} \right], \\ \langle L=1 | |[\underline{R}^{(1)} \times \underline{P}^{(1)}]^{(1)} | | L=1 \rangle &= i 3\sqrt{3}, \\ \langle L=3 | |[\underline{R}^{(1)} \times \underline{P}^{(1)}]^{(1)} | | L=3 \rangle &= i 3\sqrt{42}, \\ \langle L=1 | |[\underline{R}^{(1)} \times \underline{P}^{(1)}]^{(1)} | | L=3 \rangle &= \langle L=3 | |[\underline{R}^{(1)} \times \underline{P}^{(1)}]^{(1)} | | L=1 \rangle = 0, \\ \langle J = \frac{3}{2} | |J^{(2)} | | J = \frac{3}{2} \rangle &= 3\sqrt{30}, \\ \langle L=1 | | \underline{R}^{(2)} | | L=1 \rangle &= -6\sqrt{1/5}r^2, \\ \langle L=1 | | \underline{R}^{(2)} | | L=3 \rangle &= 3\sqrt{6/5}r^2, \\ \langle L=3 | | \underline{R}^{(2)} | | L=1 \rangle &= 3\sqrt{6/5}r^2, \\ \langle L=3 | | \underline{R}^{(2)} | | L=3 \rangle &= -2\sqrt{14/5}r^2. \end{aligned} \quad (\text{A9})$$

The matrix elements of the axial  $H_d$  terms are of the same structure. To get these matrix elements one has to substitute the spherical parameter  $\mu$  by an expression containing  $\delta$ . The following substitutions have to be made for the different  $\Delta M_L$  values:

$$\begin{aligned}\Delta M_L = 0: & \mu \rightarrow \frac{6}{5}\delta, \\ \Delta M_L = \pm 1: & \mu \rightarrow -\frac{4}{5}\delta, \\ \Delta M_L = \pm 2: & \mu \rightarrow \frac{1}{5}\delta.\end{aligned}\tag{A10}$$

- 
- <sup>1</sup>H. Venghaus, *Phys. Rev. B* **19**, 3071 (1979).  
<sup>2</sup>S. Feierabend and G. Weber, *Solid State Commun.* **26**, 191 (1978).  
<sup>3</sup>B. Sermage and G. Fishman, *Phys. Rev. B* **23**, 5107 (1981).  
<sup>4</sup>M. Aven and B. Segall, *Phys. Rev.* **130**, 81 (1963).  
<sup>5</sup>B. Segall and D. T. F. Marple, in *Physics and Chemistry of II-VI Compounds*, edited by M. Aven and J. S. Prener (North-Holland, Amsterdam, 1967).  
<sup>6</sup>D. T. F. Marple, *J. Appl. Phys.* **35**, 1879 (1964).  
<sup>7</sup>C. S. Wang and B. M. Klein, *Phys. Rev. B* **24**, 3393 (1981).  
<sup>8</sup>M. Sondergeld, *Phys. Status Solidi B* **81**, 253 (1977); **81**, 451 (1977); M. Sondergeld and R. G. Stafford, *Phys. Rev. Lett.* **35**, 1529 (1975).  
<sup>9</sup>J. M. Luttinger and W. Kohn, *Phys. Rev.* **97**, 869 (1955); J. M. Luttinger, *ibid.* **102**, 1030 (1956).  
<sup>10</sup>R. Dinges, D. Fröhlich, B. Staginnus, and W. Staude, *Phys. Rev. Lett.* **25**, 922 (1970).  
<sup>11</sup>T. C. Damen, V. T. Nguyen, and E. Gornik, *Solid State Commun.* **24**, 179 (1977).  
<sup>12</sup>D. G. Seiler, D. Heiman, R. Feigenblatt, R. L. Aggarwal, and B. Lax, *Phys. Rev. B* **25**, 7666 (1982).  
<sup>13</sup>D. Fröhlich and M. Sondergeld, *J. Phys. E* **10**, 761 (1977).  
<sup>14</sup>M. Altarelli and N. O. Lipari, *Phys. Rev. B* **7**, 3798 (1973).  
<sup>15</sup>A. Baldereschi and N. O. Lipari, *Phys. Rev. B* **8**, 2697 (1973).  
<sup>16</sup>Ch. Uihlein, D. Fröhlich, and R. Kenklies, *Phys. Rev. B* **23**, 2731 (1980).  
<sup>17</sup>A. R. Edmonds, *Angular Momentum in Quantum Mechanics* (Princeton University Press, Princeton, New Jersey, 1960); A. Messiah, *Quantum Mechanics* (North-Holland, Amsterdam, 1961).  
<sup>18</sup>H. J. Mattausch and Ch. Uihlein, *Phys. Status Solidi B* **96**, 189 (1979).  
<sup>19</sup>H. W. Hölscher, A. Nöthe, and Ch. Uihlein, *Physica* **117&118B**, 395 (1983).  
<sup>20</sup>P. Lawaetz, *Phys. Rev. B* **4**, 3460 (1971).  
<sup>21</sup>D. J. Dunstan, J. E. Nicholls, B. C. Cavenett, and J. J. Davies, *J. Phys. C* **13**, 6409 (1980).  
<sup>22</sup>B. C. Cavenett and W. E. Hagston, *Solid State Commun.* **16**, 1235 (1975).